Original Article

Influence of ZrO_2 addition on nickel aluminide layers on pure nickel substrate prepared by pack cementation

Sirichai Leelachao*, Thamvee Manochayakorn, Yasinthon Chanapol, and Patama Visuttipitukul

Department of Metallurgical Engineering, Faculty of Engineering,
Chulalongkorn University, Pathumwan, Bangkok, 10330 Thailand

Abstract

This study aims to apply pack aluminization which contains ZrO_2 powder to develop Ni_xAl_y layers on the surface of pure Ni substrate to investigate the effect of ZrO_2 content on phase development and oxidation behavior of the aluminized Ni. The surface of pure Ni substrate was aluminized at 1,000 °C for 6.25 hrs using a pack-cementation with three ZrO_2 contents in the pack mixture. Aluminized specimens were subjected to cyclic oxidation with air-cooling in ambient air at 1,000 °C. A scanning electron microscope equipped with energy-dispersive X-ray spectroscopy and an X-ray diffractometer (XRD) were used for phase analyses. Layers of coatings consisted β-NiAl, γ'-Ni3Al and Al-alloyed γ-Ni. Thicknesses decreased with increasing ZrO_2 contents. Incorporated Zr was in the forms of intermetallics. The absence of δ-Ni_2Al_3 indicated a reduction of diffusing Al activity. While the specimen with moderate ZrO_2 content showed parabolic oxidation kinetics, the multiple linear kinetics along with the high-exponent power-law oxidation were observed in the oxidized specimens prepared at other conditions. The addition of ZrO_2 in pack aluminization enables a modification of the thermodynamic Al activity. The stable α-Al_2O_3 formation was found to be promoted by the Zr addition rather than a higher Al concentration of aluminides.

Keywords: pack aluminization, diffusion coatings, thermodynamic activity, reduction reaction, zirconium-containing intermetallics, high-temperature oxidation

1. Introduction

Nickel and its alloys are usually used in petrochemical pipelines, power plants and turbine blades due to the intrinsic excellent melting point and machinability when compared with other heat-resistant materials. Oxidation at elevated temperature services of such alloys can be suppressed by an increment of surface Al-concentration using the technique called aluminization. Not only is a pack-cementation aluminizing cost-effective, but it also allows us to modify a chemical reactivity of diffusing species by simply adjusting pack mixture which result in different phase evolution obtained. Among nickel aluminides, δ-Ni_2Al_3 is problematic due to its brittleness (Donachie & Donachie, 2002) High-temperature aluminization is proposed for suppressing the formation of δ-Ni_2Al_3 which relies on a

principle of Al-activity reduction (Bose, 2018; Erdeniz & Dunand, 2014). Polymorphism of Al_2O_3 is known for inducing cracks in the protective films, resulting in a deterioration of oxidation resistance of alumina-forming alloys (Lamouri *et al.*, 2017). Thus, an alloying with zirconium in which accelerates the formation of stable α-Al_2O_3 may overcome the problem (Erdeniz & Dunand, 2014; Kim, Shang, Li, Gleeson, & Liu, 2019; White & Weaver, 2019; Zhou *et al.*, 2017). It is due to a negative energy difference of the following reduction reaction, i.e. $4Al + 3ZrO_2 = 3Zr + 2Al_2O_3$, at temperature ≤ 700°C (Zare Mohazabie & Shahriari Nogorani, 2019). According to the reaction that 4/3 moles of Al would be consumed for producing one mole of Zr. Not only is a simultaneous addition of Zr into aluminide coatings possible for pack aluminization which consisting of Al and ZrO_2 powder as ingredients, the thermodynamic activity of diffusible Al-rich species can be also modified.

To investigate a correlation between ZrO_2 content in the pack with a formation of nickel aluminides and their oxidation behaviors, we therefore aim to investigate on the Zr-

*Corresponding author
Email address: sirichai.l@chula.ac.th

modified aluminized commercially pure Ni with lower content of ZrO_2 powder.

2. Materials and experimental

2.1 Aluminizing process

All chemicals used in experiments were commercial-grade except ZrO_2 powder which was analytical-grade (Riedel-de Haën, Germany). Compositions in pack mixture containing Al, NH_4Cl, Al_2O_3, and ZrO_2 powders were listed in Table 1. A nominal atomic ratio presented in Table 1 is estimated from the remaining amount of Al in the packs and obtained Zr atoms after the reduction reaction fully completed. Commercially pure nickel strips (Kenis, Japan) were cut with dimensions $15 \times 15 \times 0.3$ mm^3 whose surfaces were polished using 1,000-grit abrasive papers. After being ultrasonically cleaned in acetone, substrates were vertically embedded into the mixture in separate alumina crucibles. Additional Al_2O_3 powder was added on top of the pack to fill up the crucible. Air-setting refractory mortar was used as a sealant to an alumina lid. A schematic of the crucible setup is illustrated in Figure 1a.

All crucible was placed in a horizontal furnace to perform aluminization at the same time where a temperature profile is displayed in Figure 1b. Adsorbed moisture was removed by baking at 100 °C for 10 min followed by the aluminizing process at 1,000 °C for 6.25 hrs. The heating rate was constant at 5 °C·min^{-1}. A quartz reactor was purged with industrial Ar gas (99.5%-purity, Linde, Thailand) at a rate of 3 L·min^{-1} from the beginning to a cool-down stage at a temperature of about 600 °C; the crucible was then furnace-cooled to room temperature. Aluminized samples were dissected using a Struers Accutom-5 precision cutting machine. Microstructure and phase identification of diffusion layers were examined using a JOEL JSM-IT100 scanning electron microscope equipped with an energy dispersive spectroscope (SEM-EDS) and a Bruker D8 Advance X-ray

diffractometer (XRD) using Cu Kα source, respectively. By excluding Ni from quantitative EDS mapping scans, an average atomic fraction of Al and Zr in three different locations of the coatings was used to determine the incorporated Zr concentration.

2.2 Cyclic oxidation experiments

Cyclic oxidation was performed using a box furnace at 1,000 °C for 8 hrs per cycle under an ambient atmosphere. Alumina boats containing each specimen were inserted at room temperature into a preheated furnace to avoid the effect of the heating period. After 8 hrs of oxidation, the specimens were subjected to an air quenching to aggravate the failure of oxides. Weight change was measured using an OHAUS PA214 analytical balance without removing the specimen from the boat. Oxidized layers were analyzed using a Rigaku D/Max 2200P/C glancing incident angle X-ray diffractometer (GIXRD) at an incident angle of 3° using a parallel Cu Kα beam whereas their topography was examined using a Hitachi S4800 scanning electron microscope.

ICSD numbers used for phase identification are listed as follow: Pure Ni (#004-0850), β-NiAl (#044-1188), γ'-Ni$_3$Al (#009-0097), α-Al$_2$O$_3$ (#046-1212), θ-Al$_2$O$_3$ (#023-1009), γ-Al$_2$O$_3$ (#050-0741), δ-Al$_2$O$_3$ (#046-1215), NiAl$_2$O$_4$ (#010-0339) and NiO (#044-1159).

3. Results and Discussion

3.1 Phase evolution of the aluminized specimens

Back-scattered SEM images reveal the difference in microstructural development. The coatings with Kirkendall voids from the Zr10 (Figure 2a) composed of chemical compositions in each sublayer, listed in Table 2, that correspond to the following sequence: (1) Stoichiometric β-NiAl, (2) Ni-rich β-NiAl, (3) γ'-Ni$_3$Al and (4) Al-dissolved γ-Ni, accordingly. The faded boundary between the

Table 1.   Pack compositions used for Zr-doped aluminization. Nominal atomic fraction is calculated from theoretical value of the reduced Zr and the remained Al atoms based on 4Al + 3ZrO2 = 3Zr + 2Al2O3.

Specimen	Nominal atomic fraction Zr/(Zr+Al)	Al powder (wt.%)	ZrO$_2$ powder (wt.%)	NH4Cl powder (wt.%)	Al2O3 powder (wt.%)
Zr10	10%	13.87	6.13	4.00	76.00
Zr20	20%	10.78	9.22	4.00	76.00
Zr30	30%	8.91	11.09	4.00	76.00
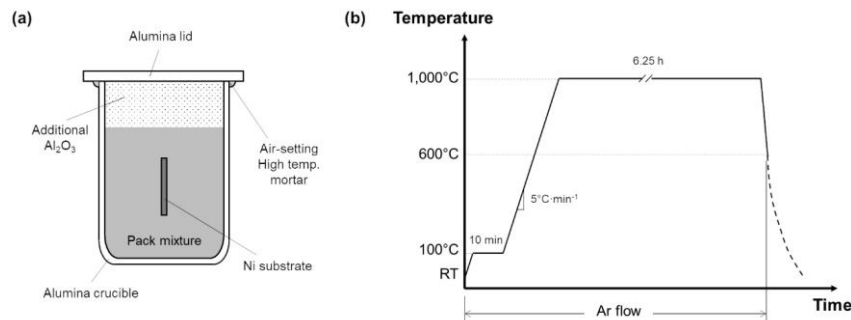
Figure 1.   (a) Crucible setup and (b) temperature profile used in the study
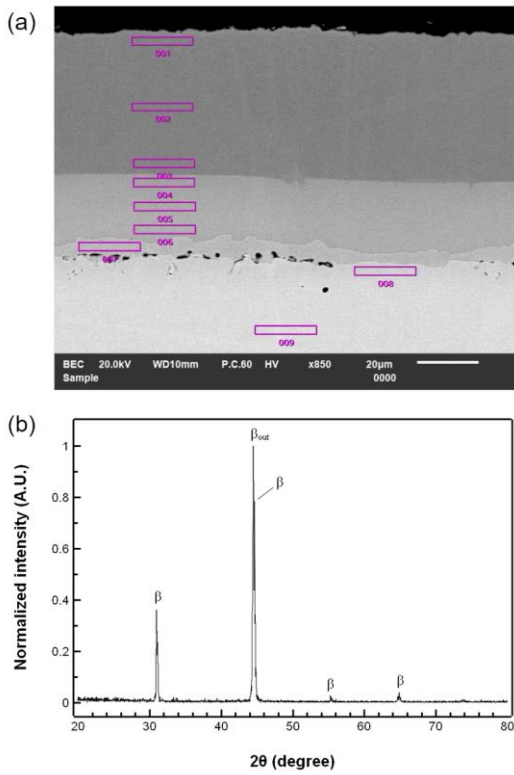
Figure 2.　(a) Cross-sectional image and (b) X-ray diffraction patterns of the as-prepared Zr10. Symbol β is assigned to β-NiAl

stoichiometric and the Ni-rich β-NiAl layer is suggested to be due to a competitive diffusion (Bozza *et al.*, 2014) as the layer

of β-NiAl with a disproportionate Ni content was observed which might be due to large difference in Ni diffusivity in β-NiAl (Shankar & Seigle, 1978). Diffraction patterns of the Zr10 showed consistent predominate β-NiAl phase as shown in Figure 2b. It is noteworthy mentioning that no Zr was incorporated in the specimen which might be due to two reasons: (i) multiple species of zirconium chlorides ($ZrCl_4$, $ZrCl_3$, $ZrCl_2$, ZrCl) than those of aluminium ($AlCl_3$, $AlCl_2$, AlCl) are possible so that a disproportionation reaction is hindered, and (ii) an efficiency of reactions are not 100% as can be seen that the obtained Zr concentration in the coatings was lower than the nominal values.

As the content of ZrO_2 increased, the coatings were visually changed into the bilayered structure with bright precipitates appeared where Kirkendall voids and the thickness of the coatings were significantly reduced. Fraction of the precipitates was significantly higher for the Zr30 specimen, as compared in Figure 3a and 3b. Regarding EDS

Table 2.　Elemental concentrations of corresponding points of the Zr10 where the point No. is referred to those of Figure 2a.

Point No.	Ni (at.%)	Al (at.%)	Zr (at.%)	Suggested phase(s) according to (Chen *et al.*, 2013)
001	48.63	51.37	0.00	β-NiAl
002	49.03	50.97	0.00	
003	50.13	49.87	0.00	
004	61.64	38.36	0.00	Ni-rich β-NiAl
005	64.67	35.33	0.00	
006	66.31	33.69	0.00	
007	78.09	21.91	0.00	γ'-Ni₃Al
008	92.27	7.73	0.00	Al-dissolved γ-Ni
009	100.00	0.00	0.00	γ-Ni substrate
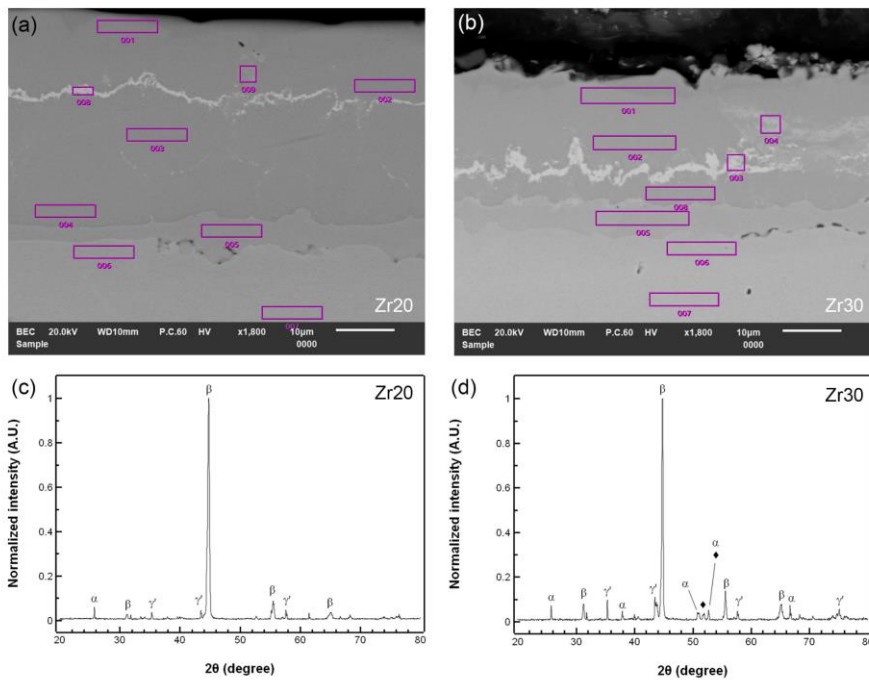
Figure 3.　Microstructures of the aluminized layers of (a) Zr20 and (b) Zr30 along with corresponding X-ray diffractograms of (c) Zr20 and (d) Zr30, respectively

results of the Zr20 and the Zr30, as shown in Table 3 and 4, respectively, while constituents of the coatings were identical to those of the Zr10, Ni-rich β-NiAl layer was predominant with a thin layer of the stoichiometric β-NiAl layer. As expected from distinguishable contrast, the precipitates contained a higher amount of Zr whose composition was assigned to be Ni_7Zr_2. For the Zr30, a ternary intermetallic $AlNi_2Zr$ were observed fainted regions, as represented in Spectrum 4 in Figure 3b, along with Ni_7Zr_2 and β-NiAl. Similarly, the x-ray diffractograms of both conditions (Figure 3c and 3d) were in accordance with the suggested phases. Noticeable Al_2O_3 peaks might indicate the outward layer growth (Mohseni Bababdani & Shahriari Nogorani, 2014). As illustrated in Figure 4, the presence of two distinctive β-NiAl layers with different compositions can be demonstrated as the separated (110) peak around 44.5°- 44.8°. The total thickness of the coatings was decreased with increasing the ZrO_2 content in the pack whereas the incorporated Zr concentration in the coatings was found to be lower than that of the theoretical value as shown in Figure 5. According to the results, it emphasizes the possibility of the reaction between ZrO_2 and Al powders during aluminization whose conversion was restricted. Not only is the thermodynamic activity of aluminum modified as indicated by the thickness reduction and Ni-rich β-NiAl phase, the incorporation of Zr atoms can be also achieved which presented as intermetallic precipitates which might be due to either a limited solubility (Chen, Huang, Liu, Zheng, & Jin, 2013; Noebe, Bowman, & Nathal, 1996) or a slow diffusivity of Zr (Wierzba, Romanowska, Zagula-Yavorska, Markowski, & Sieniawski, 2015) in nickel aluminides.

Table 3.   Elemental concentrations of corresponding points of the Zr20 where the point No. is referred to those of Figure 3a.

Point No.	Ni (at.%)	Al (at.%)	Zr (at.%)	Suggested phase(s) according to (Chen *et al.*, 2013)
001	60.34	39.66	0.00	β-NiAl
002	64.04	35.96	0.00	Ni-rich β-NiAl
003	65.35	34.65	0.00	
004	65.69	34.31	0.00	
005	78.22	21.78	0.00	γ'-Ni_3Al
006	89.64	10.36	0.00	Al-dissolved γ-Ni
007	100.00	0.00	0.00	γ-Ni substrate
008	63.63	32.19	4.18	β-NiAl+ Ni_7Zr_2
009	59.90	34.56	5.54	

Table 4.   Elemental concentrations of corresponding points of the Zr30 where the point No. is referred to those of Figure 3b.

Point No.	Ni (at.%)	Al (at.%)	Zr (at.%)	Suggested phase(s) according to (Chen *et al.*, 2013)
001	57.03	42.97	0.00	β-NiAl
002	63.20	36.80	0.00	Ni-rich β-NiAl
008	65.32	34.68	0.00	
003	62.71	22.08	0.00	Ni-rich β-NiAl + Ni_7Zr_2
004	51.58	30.14	0.00	Ni-rich β-NiAl + Ni_7Zr_2 + $AlNi_2Zr$
005	78.32	21.68	0.00	γ'-Ni_3Al
006	92.35	7.65	0.00	Al-dissolved γ-Ni
007	100.00	0.00	0.00	γ-Ni substrate
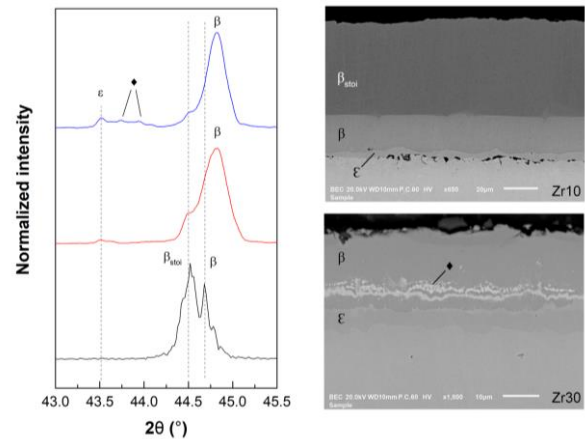
Figure 4.   Peak separation at 44.5° confirms an existence of a stoichiometric β-NiAl ($β_{stoi}$) as the outer layer in the Zr10-specimen. Different chemical compositions of the Ni-rich NiAl layer (β) contributes to a peak shift.
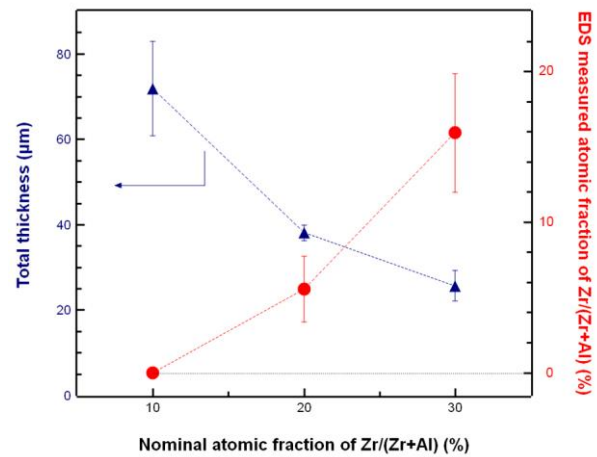
Figure 5.   Correlation of the expected Zr concentration on thicknesses of the coatings (▲) and the obtained Zr/(Zr+Al) measured by EDS mappings analyses which excluded Ni (●).

3.2 Oxidation behavior of the aluminized specimens

Specific mass gain of different ZrO_2 content aluminized specimens is shown in Figure 6. The lowest oxidation rate was observed for the Zr20 with parabolic kinetics. While the Zr10 specimen shows a two-step linear oxidation with a transition time of 24 hrs, the Zr30 shows three steps, with the first two exhibiting linear kinetics with an earlier transition at 16 hrs, followed by power-law oxidation behavior. Evidently, the detrimental effect of excessive Zr additions is demonstrated. Calculated rate constants are listed in Table 5. Equation 1 was used to determine an exponent (n) and a rate constant (k_w) of the power-law oxidation where Δm is a mass gain and τ is a transition time of 40 hrs,

$$\Delta m = k_w(x-\tau)^n + b \qquad (1)$$

Oxide evolution is demonstrated by XRD patterns of the oxidized specimens at 24 hrs and 80 hrs of oxidation times. At the early stage of oxidation (Figure 7a-7c), a
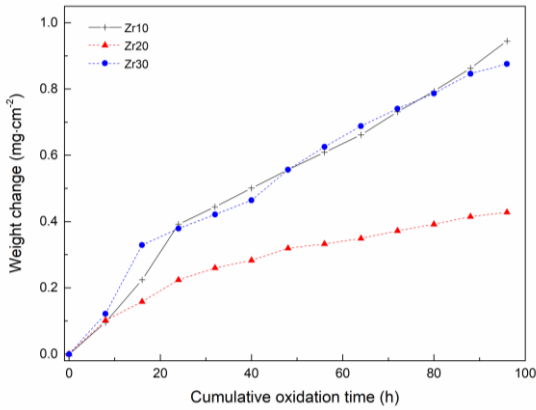
Figure 6. Mass change of Zr10 (+), Zr20 (▲) and Zr30 (●) subjected to a cyclic oxidation at 1,000°C with rapid heating and quenching. Arrows indicate the XRD measurements at 24 h- and 80 h-oxidation.

Table 5. Calculated rate constants from corresponding oxidation times

Sample	Oxidation period (h)	Kinetics and its exponent	Calculated rate constants
Zr10	0-24	Linear	$k_l = 1.63 \times 10^{-2}$ mg·cm^{-2}·h^{-1}
	24-96	Linear	$k_l = 7.54 \times 10^{-3}$ mg·cm^{-2}·h^{-1}
Zr20	0-96	Parabolic (n=0.503)	$k_p = 1.94 \times 10^{-2}$ mg^2·cm^{-4}·h^{-1}
Zr30	0-16	Linear	$k_l = 2.06 \times 10^{-2}$ mg·cm^{-2}·h^{-1}
	16-40	Linear	$k_l = 5.60 \times 10^{-3}$ mg·cm^{-2}·h^{-1}
	40-96	Power law (n=0.750)	$k_W = 2.06 \times 10^{-2}$ mg$^{4/3}$·cm$^{-8/3}$·h^{-1}

significant fraction of transient θ- and γ-Al$_2$O$_3$ was observed for the oxidized Zr10 as being compared to other conditions. Transient θ-Al$_2$O$_3$ was undetected in the oxidized Zr20. Additionally, Al in aluminides was gradually consumed, resulting in a transformation of Ni-rich β-NiAl into γ'-Ni$_3$Al.

As the oxidation proceeded, the effect of Zr incorporation in the coatings took place. While transient alumina were still major constituents for the oxidized Zr10 (Figure 7d), the stable α-Al$_2$O$_3$ was suggested to be predominant with remaining γ'-Ni$_3$Al for the Zr20 and the Zr30 specimens (Figure 7e-7f). Oxide scale of the Zr10 subjected to 96 hrs of oxidation (Figure 8a) exhibited cracks and θ-Al$_2$O$_3$ needles on the rugged surface while the oxidized Zr30 (Figure 8c) showed cracks and delaminated patches composing of finer θ-
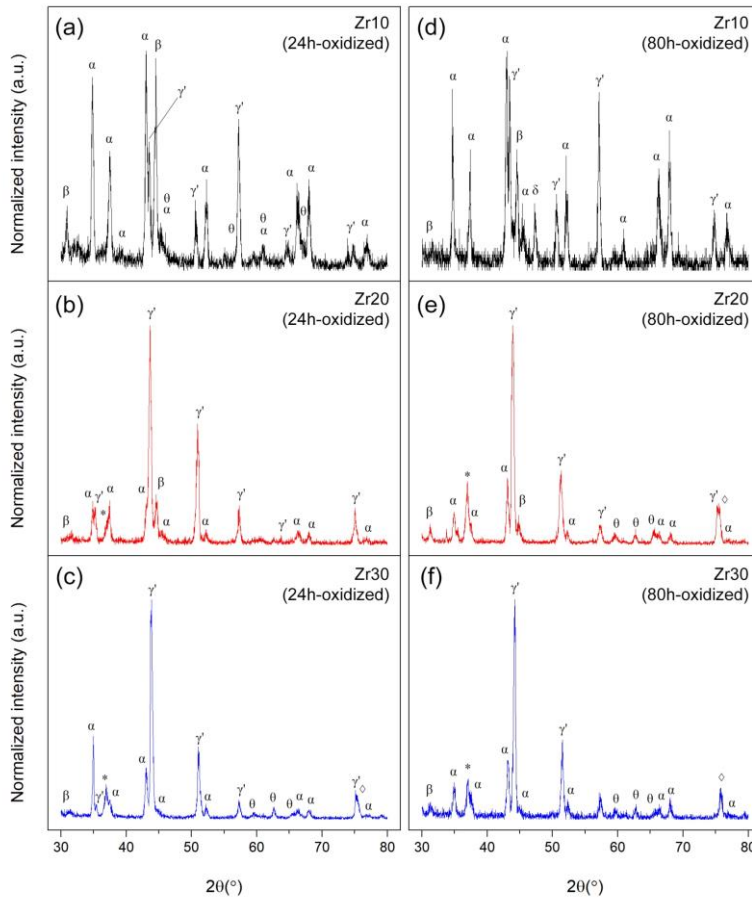
Figure 7. XRD spectra after 24 hrs of cyclic oxidation of (a) Zr10, (b) Zr20 and (c) Zr30; 80 hrs of cyclic oxidation of (d) Zr10, (e) Zr20 and (f) Zr30. Each symbol is assigned as follows: α = α-Al$_2$O$_3$, β = NiAl, γ' = Ni$_3$Al, θ = θ-Al$_2$O$_3$, γ = γ-Al$_2$O$_3$, δ = δ-Al$_2$O$_3$, * = NiAl$_2$O$_4$ and ◇ = NiO.

Al_2O_3 needles; the patch-like structure observed in the study is comparably similar to ridges or cellular oxide scale caused by Zr-rich precipitates reported in (Doychak, Smialek, & Barrett, 1988). Observed cracks put a direct emphasis on their linear oxidation behaviors (Davis, 1997; Khanna, 2013). Rapid and slow linear oxidation kinetics in the Zr10 specimen formation of θ-Al_2O_3 and α-Al_2O_3, respectively, as the transient shows a higher growth rate (Brumm & Grabke, 1992). For the oxidized Zr30, two first linear oxidations might also involve alumina formations and cracks since the corresponding rate constants are in the same order of magnitude as those of the oxidized Zr10. As shown in Figure 8d, a smooth surface topography underneath the spiked patches suggested two different Al_2O_3, at least, were involved. It might be relevant to the power-law oxidation with a higher exponent than 0.5 which implies a simultaneous oxidation behavior. The results indicate that higher Al concentration does not always be beneficial for oxidation resistance of aluminides whereas a formation of stable α-Al_2O_3 can be manipulated by incorporated Zr.

On the other hand, the scale from the oxidized Zr20 (Figure 8b) is composed of nodular α-Al_2O_3 with coarser needles of θ-Al_2O_3 with a smoother surface where cracks are not observed. This might correspond to a formation of a continuous protective layer whose oxidation kinetic is parabolic (Davis, 1997; Khanna, 2013). Calculated parabolic rate constant k_p is in good agreement with either the upper bound α-Al_2O_3 formation from a stoichiometric β-NiAl (Noebe *et al.*, 1996) or the reported value for ϵ-Ni_3Al (Lee & Santella, 2004). In this study, a formation of α-Al_2O_3 is likely to originate from Ni-rich β-NiAl layer. Substantial low oxidation behavior of the Zr20 specimen whose parabolic rate constant at 1.94×10^{-2} $mg^2 \cdot cm^{-4} \cdot h^{-1}$, which is in good agreement with the reported rate constant of Zr-doped NiAl

alloys (An, Guan, Sun, & Hu, 2000), emphasizes on a formation of nodular α-Al_2O_3 while the needle-like transient θ-Al_2O_3 was suppressed. Continuous Zr-rich precipitates may play an important role for a uniform supply of Zr during oxidation. The detrimental effect of excessive Zr on oxidation behavior of nickel aluminides were also reported (Zhou *et al.*, 2017) as the result of internal oxidation (Kaplin & Brochu, 2011).

4. Conclusions

An addition of ZrO_2 powder into pack aluminizing mixtures directly reduces the thermodynamic Al activity which facilitates a formation of β-NiAl phase without post-process treatment along with a decrease in thickness of the coatings. Conversion of reduction reaction is limited so that a sufficient ZrO_2 content in the pack is essential for incorporating Zr where a recommended ratio of ZrO_2 and Al powder in the pack is suggested to be greater than 1:1, according to this study. Zr is rather found in intermetallics, suggesting low solubility in Ni_xAl_y or sluggish diffusion of Zr. Higher Al concentration of aluminides does not attribute to an α-Al_2O_3 formation. The lowest oxidation rate with parabolic kinetics is achieved when a weight ratio of ZrO_2 to Al at 1:1 where the excessive Zr incorporating concentration is found to have an adverse alumina scale formation.

Acknowledgements
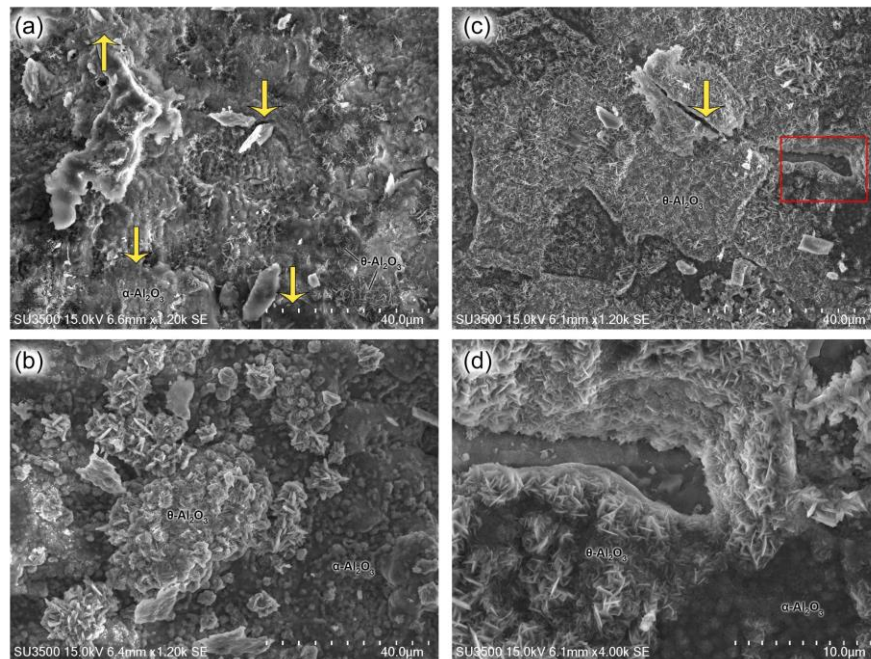
Figure 8. Oxide scale topography of the 96h-oxidized (a) Zr10, (b) Zr20, (c) Zr30 and (d) higher magnification of the selected area in the oxidized Zr30. Cracks are addressed by arrows.

References

An, T. F., Guan, H. R., Sun, X. F. & Hu, Z. Q. (2000). Effect of the θ–α-Al$_2$O$_3$ transformation in scales on the oxidation behavior of a nickel-base superalloy with an aluminide diffusion coating. *Oxidation of Metals*, 54(3/4), 301–316. doi:10.1023/A:1004654429687

Bose, S. (2018). *High temperature coatings*. Oxford, England: Butterworth-Heinemann.

Bozza, F., Bolelli, G., Giolli, C., Giorgetti, A., Lusvarghi, L., Sassatelli, P., . . . Thoma, M. (2014), Diffusion mechanisms and microstructure development in pack aluminizing of Ni-based alloys. *Surface and Coatings Technology*, 239, 147-159. doi:10.1016/j.surfcoat.2013.11.034

Brumm, M. W., & Grabke, H. J. (1992). The oxidation behaviour of NiAl-I. Phase transformations in the alumina scale during oxidation of NiAl and NiAl-Cr alloys. *Corrosion Science*, *33*(11), 1677-1690. doi:10.1016/0010-938X(92)90002-K

Chen, Q., Huang, L. H., Liu, H. S., Zheng, F., & Jin, Z. P. (2013). Isothermal sections of Al-Ni-Zr ternary system at 850 and 1050°C. *Journal of Phase Equilibria and Diffusion*, *34*(5), 390-402. doi:10.1007/s11669-013-0248-8

Davis, J. R. (1997). *ASM specialty handbook: Heat-resistant materials*. Novelty, OH: ASM International.

Donachie, M. J., & Donachie, S. J. (2002), *Superalloys: A technical guide (2nd ed.)*. Novelty, OH: ASM International.

Doychak, J., Smialek, J. L., & Barrett, C. A. (1988). *The oxidation of Ni-rich Ni-Al intermetallics* (NASA TM-101455).

Erdeniz, D., & Dunand, D. C. (2014). Microstructure development during pack aluminization of nickel and nickel–chromium wires. *Intermetallics*, *50*, 43-53. doi:10.1016/j.intermet.2014.02.009

Kaplin, C., & Brochu, M. (2011), Effects of water vapor on high temperature oxidation of cryomilled NiCoCrAlY coatings in air and low-SO$_2$ environments. *Surface and Coatings Technology,* *205*(17–18), 4221-4227. doi:10.1016/j.surfcoat.2011.03.026

Khanna, A. S. (2013). High-temperature oxidation. In M. Kutz (Ed.), *Handbook of environmental degradation of materials* (2nd ed., pp. 127-194). Berlin, Germany: Elsevier.

Kim, D., Shang, S., Li, Z., Gleeson, B., & Liu, Z.-K. (2019). Effects of Hf, Y, and Zr on alumina scale growth on NiAlCr and NiAlPt alloys. *Oxidation of Metals*, *92*(3), 303-313. doi:10.1007/s11085-019-09928-8

Lamouri, S., Hamidouche, M., Bouaouadja, N., Belhouchet, H., Garnier, V., Fantozzi, G., & Trelkate, J.F. (2017). Control of the γ-alumina to α-alumina phase transformation for an optimized alumina densification. *Boletín de la Sociedad Española de Cerámica y Vidrio*, *56*(2), 47-54. doi:10.1016/j.bsecv.2016.10.001

Lee, D. B., & Santella, M. L. (2004). High temperature oxidation of Ni$_3$Al alloy containing Cr, Zr, Mo, and B. *Materials Science and Engineering: A*, *374(1)*, 217-223. doi:10.1016/j.msea.2004.02.012

Mohseni Bababdani, S., & Shahriari Nogorani, F. (2014). Overaluminizing of a CoNiCrAlY coating by inward and outward diffusion treatments. *Metallurgical and Materials Transactions A*, *45*, 2116–2122. doi:10.1007/s11661-013-2138-4

Noebe, R. D., Bowman, R. R., & Nathal, M. V. (1996). The physical and mechanical metallurgy of NiAl. In N. S. Stoloff & V. K. Sikka (Eds.), *Physical metallurgy and processing of intermetallic compounds* (pp. 212-296). Boston, MA: Springer.

Shankar, S., & Seigle, L. L. (1978). Interdiffusion and intrinsic diffusion in the NiAl (δ) phase of the Al-Ni system. *Metallurgical Transactions A*, *9*(10), 1467-1476. doi:10.1007/BF02661819

White, R., & Weaver M. (2019). Microstructural investigation of the thermally grown oxide on grain-refined overdoped NiAl–Zr. *Oxidation of Metals*, *92*(3), 227-242. doi:10.1007/s11085-019-09920-2

Wierzba, B., Romanowska, J., Zagula-Yavorska, M., Markowski, J., & Sieniawski, J. (2015). The Ni-Al-Zr multiphase diffusion simulations. *High Temperature Materials and Processes*, *34*(5), 495-502. doi:10.1515/htmp-2014-0080

Zare Mohazabie, M. S., & Shahriari Nogorani, F. (2019). The addition of zirconium to aluminide coatings: The effect of the aluminide growth mode. *Surface and Coatings Technology*, *378*(25), 125066-1-8. doi:10.1016/j.surfcoat.2019.125066

Zhou, Y., Zhao, X., Zhao, C., Hao, W., Wang, X., & Xiao, P. (2017). The oxidation performance for Zr-doped nickel aluminide coating by composite electro depositing and pack cementation. *Corrosion Science*, *123*, 103-115. doi:10.1016/j.corsci.2017.04.00